Asian Journal of Chemistry; Vol. 36, No. 3 (2024), 661-668

ASIAN JOURNAL OF CHEMISTRY

https://doi.org/10.14233/ajchem.2024.31124

ERGO-based Bimetallic Nanocomposite as Novel Sensing Material for the Assay of 4-Nitrophenol in Water Samples

K. Gowri Bala Kumari[1], T.V. Reddy[2], Akkaraboyina Lakshmi Lavanya[3] and T.N.V.S.S. Satyadev[4,*]

[1]Department of Chemistry, Acharya Nagarjuna University, Nagarjuna Nagar-522502, India
[2]Department of Chemistry, Mallareddy College of Engineering, Secunderabad-500100, India
[3]Department of Chemistry, Aditya College of Engineering, Surampalem-533437, India
[4]Department of Chemistry, P.B. Siddhartha College of Arts and Science, Moghalrajpuram, Vijayawada-520010, India

*Corresponding author: E-mail: satyadev2satya@gmail.com

Received: 21 December 2023; *Accepted*: 1 February 2024; *Published online*: 28 February 2024; AJC-21559

A new approach for detecting and quantifying *p*-nitrophenol, a major environmental pollutant, is the focus of this work, which involves the electrochemical fabrication of a bimetallic alloy of ruthenium and nickel on an ergo-based pencil graphite electrode. The characterization of the fabricated composite involves techniques such as X-ray diffraction, scanning electron microscopy (SEM) and energy-dispersive X-ray spectroscopy (EDS). The composite was observed to form clusters with a size of 4.30 nm. The electrooxidation of *p*-nitrophenol on the Ru@Ni/ERGO/PGE electrode was investigated using chronoamperometric studies. The results indicate a satisfactory linear relationship between *para*-nitrophenol concentration within the range of 2.5 to 50 µM. Significantly, the proposed method demonstrates a low detection limit of 0.36 µM and a limit of quantification of 1.1×10^{-6} M. The nanocomposite electrode exhibits favourable outcomes in terms of selectivity, sensitivity and repeatability for an electrochemical sensor material. Stability testing conducted over five weeks further supports the reliability of the electrode. The capability of sensor is validated in real samples including soil and water. This study introduces a promising electrochemical sensor material in the composite electrode making it more effective in detecting *p*-nitrophenol.

Keywords: Ruthenium and Nickel alloy, Nickel, ERGO, Pencil graphite electrode, *p*-Nitrophenol, Electrochemical sensor.

INTRODUCTION

Nitrophenols are a significant intermediary compound within several industrial processes, particularly in waste streams produced by mining, paint, petrochemical and pharmaceutical sectors. These compounds can potentially pose health hazards such as methemoglobinemia, inflammation and allergy responses in both human and animal subjects. In addition, it should be noted that mono-aromatic compounds could undergo interactions with nitrogen oxides and ozone within the troposphere. This interaction leads to the formation of nitrophenols, which have been observed to be present in rainfall at a concentration of roughly 170 nM. The acute inhalation or ingestion of *p*-nitrophenol in humans results in symptoms such as headaches, sleepiness, nausea and cyanosis, which is characterized by a blue discolouration in the lips, ears and fingernails. As per the guidelines provided by the World Health Organization (WHO), the acceptable level of phenolic contents in drinking water is 1 µg dm^{-3}. The classification of nitrophenols as dangerous priority harmful pollutants has been undertaken by the U.S. Environmental Protection Agency. Therefore, there is a growing emphasis on treating effluents containing nitrophenol to protect the environment [1-5].

The literature survey reveals that several alternative methods have been employed for the analysis of *p*-nitrophenol in water samples. These techniques include fluorimetry [6], HPLC, colorimetry [7,8], UV-visible spectrophotometry [9] and voltammetry [10-12]. Currently, there is a strong focus on creating nanocomposite materials that can serve as effective and cost-efficient sensors in the field of analytical chemistry [13]. Several electrodes have been prominently utilized, including the carbon paste electrode [14], glassy carbon electrode [15], screen printed electrode [16], pencil graphite electrode [17], paper electrode and carbon cloth electrode [18]. Pencil graphite electrodes (PGE) and their associated sensors have attracted considerable attention in the field of electroanalysis, exceeding alternative

solid-state electrodes. The practical advantages of this can be ascribed to its large potential range, uncomplicated manufacturing process and cost-efficient techniques of customization [19,20].

In literature, various types of dimensionally stable anodes have been extensively studied for their potential application in wastewater treatment. These include immediate boron doped diamond [21], titanium coated with metal oxides such as RuO_2 [22], ZnO [23], PbO_2, TiO_2 [24]. Transition metals, including ruthenium, tantalum, iridium, tin, antimony, nickel, cobalt [25] and others, have been identified as suitable anode materials. RuO_2 exhibits exceptional stability and possesses remarkable mechanical and chemical resilience, particularly when subjected to intense acidic environments, in comparison to other metal oxides.

Extensive studies have been conducted on the geometric and electrical properties of bimetallic nanoparticles, characterized by the presence of two distinct metals arranged in random alloys, segregated configurations or core-shell architectures. It is crucial to comprehend that the disparities among metals concerning their fundamental properties, such as ionization potentials, electronegativities and work functions, exert a substantial influence on the interactions between neighbouring metals. Hence, the properties of bimetallic nanoparticles, as well as their size control, are determined by their elements' composition. In addition to exhibiting distinctive synergistic properties, the partial replacement of costly noble metals with more affordable metals holds significant economic significance [26].

Graphene, a 2D structure, possesses a range of oxygen functional groups, including hydroxyl and epoxy, distributed over its surface. Graphene oxide is commonly employed for electrode alterations owing to its advantageous characteristics, including favourable electrical conductivity, elevated mechanical strength, expansive specific surface area and exceptional electrocatalytic capabilities. To date, no method has been identified that effectively employs pencil graphite electrodes, namely those that are coated with electrochemically synthesized bimetallic alloy.

EXPERIMENTAL

All the chemicals, *viz.* potassium chloride, nickel chloride, ruthenium trichloride, potassium dichromate, potassium ferrocyanide, potassium ferricyanide, sodium dihydrogen phosphate, disodium hydrogen phosphate, hydrochloric acid and sulfuric acid were obtained from Sigm-Aldrich, USA and used as received. All solutions were prepared in deionized water.

The electrochemical analysis was conducted using Metrohm PGSTAT Autolab equipment, model no. 204, in conjunction with NOVA software version 2.1.4. In this experiment, the Ag/AgCl electrode functions as reference electrode, the Pt electrode functions as counter electrode and the PGE electrode functions as the working electrode. The working electrode was graphite lead with a diameter of 0.7 mm obtained from Camlin Kokuyo. The experimental setup involved the utilization of the Systronic-362 pH meter, which was employed to obtain measurements. This process encompassed the incorporation of both the temperature probe and the Ag/AgCl reference electrode. The ultrasonic cleaning process was conducted using a SISCA ultrasonic cleaner for all the solutions. The identification of crystallite and size was conducted using an X-ray diffraction analysis using the Xrd_Rigaku Minillex 600 instrument manufactured by Rigaku Corporation, a Japanese company. Surface elemental analysis and morphology were performed using the EDX technique with a gun acceleration voltage of 20 kV. The analysis was conducted using an FEI Quanta FEG 200 microscope, which has an accelerating voltage range of -200 to 30 kV, a resolution of 1.2@30kV and a magnification range of 12x to 105 kx.

Synthesis of ruthenium–nickel bimetallic nanoparticles

Graphite to graphene oxide: The length of the graphite electrodes used in the experiment was 3.0 cm. The alteration process was conducted using the chronoamperometric approach. Under the optimal parameters, the working electrode was subjected to a constant potential of +1.9V for 60 s in a solution of 5.0 M sulfuric acid. Following the alteration process, the electrodes underwent a thorough cleansing procedure through immersion in pure water, subsequently being kept in a desiccator [27].

Electrochemical synthesis

Electrochemical synthesis and deposition of nickel nanoparticles: A 0.01 M Ni^{2+} solution was prepared by adding 0.2 mL of 2 M $NiCl_2$ solution to a mixture of 5 mL of 0.1 N HCl and 33.8 mL of 0.1 M KCl solution. The pH of the solution was adjusted to 1 by adding HCl/KOH. Electrodeposition of nickel was done on ERGO by cyclic voltammetry over a potential range of -0.1 V to -1 V at a scan rate of 0.05V/s for about 6 cycles.

Electrochemical synthesis and deposition of ruthenium nanoparticles: A 0.2 mL of 0.2 M $RuCl_3{\cdot}xH_2O$ was added to a mixture of 5 mL of 0.1 N HCl and 33.8 mL of 0.1 M KCl solution. The pH of the solution was adjusted to 1 by adding HCl/KOH. Electrodeposition of ruthenium nanoparticles was done on ERGO by cyclic voltammetry over a potential range of 0 V to -1.5 V at a scan rate of 0.05 V/s for about 6 cycles.

Fabrication of composite electrode: A 30 mL of 0.1 M KCl, 5 mL of 0.1 N HCl, 0.2 mL of 0.2 M $RuCl_3{\cdot}xH_2O$ and 0.2 mL of 2 M $NiCl_2$ solutions were taken in a beaker and pH of the solution was adjusted to 1 by adding HCl/KOH solution. After sonication for 5 min for the uniformity of the solution, electrodeposition is done on ERGO by cyclic voltammetry over a potential range of 0 V to -1.5 V at a scan rate of 0.05 V/s for about 6 cycles. Modified electrodes are represented as Ru@Ni/ERGO/PGE [28].

RESULTS AND DISCUSSION

Characterization of RuNPs@NiNPs/ERGO: The presence of nanoparticles on the electrode's surface was verified by the utilization of scanning electron microscopy (SEM) and energy-dispersive X-ray spectroscopy (EDX) research. The X-ray diffraction (XRD) studies confirmed the crystalline structure of the materials under consideration. The powder X-ray diffraction (XRD) patterns of the various electrode samples were obtained

by employing a diffractometer equipped with Cu*K*α radiation (λ = 1.5406 Å). Fig. 1 illustrates the X-ray diffraction (XRD) pattern which indicate the crystalline structure of ruthenium, nickel and ruthenium@nickel nanoparticles. The diffraction peaks at 38.38º, 42.28º and 44.5º are indicative of the crystallographic planes (100), (002) and (101), respectively, with *d*-spacing 2.32, 2.13 and 2.03 Å respectively to the hexagonal crystals of RuNPs/ERGO (JCPDS card no. 00-006-0663). The peaks at 2θ 44.35º and 86.94º provide clear evidence for the presence of (101) and (112) planes with *d*-spacing of 2.04 and 1.02 Å related to a hexagonal crystal lattice (JCPDS card no. 00-041-1487) of nickel. The X-ray diffraction pattern obtained from the RuNPs@NiNPs/ERGO sample exhibited prominent peaks at 2θ values of 39.6º and 45.5º with *d*-spacing 2.27 and 2.03 Å and (100) and (101) as *hkl* values corresponding to the Ru@Ni nanoparticles (JCPDS card no. 03-065-6490) [28]. The observed increase in peak intensity and minor deviation in the diffraction angle could potentially be attributed to the electrostatic interaction occurring between the metal nanoparticles and graphene oxide. The detected peak at 26.26º with a *d*-spacing value of 3.39 Å can be attributed to the existence of electrochemically reduced graphene oxide, as found in all three patterns. The calculation of crystallite size was performed using the Debye-Scherrer's formula (eqn. 1) and the size was found to be 4.30 nm.

$$D = \frac{K\lambda}{\beta \cos\theta} \quad (1)$$

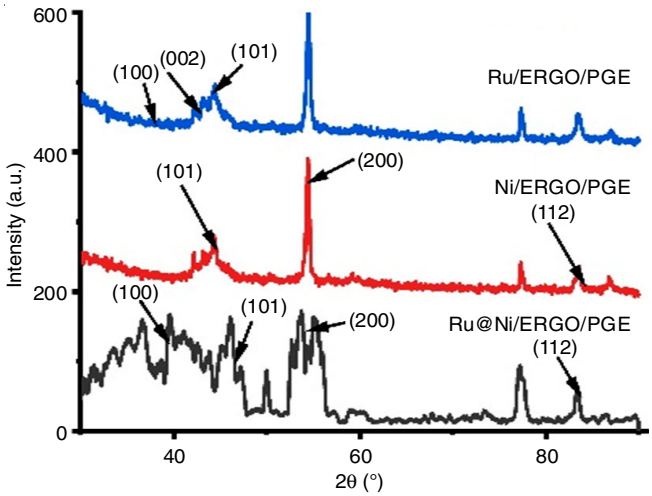

Fig. 1. XRD pattern of Ru/ERGO/PGE, Ni/ERGO/PGE and Ru@Ni/ERGO/PGE

FESEM studies: The unmodified pencil graphite electrode and other modified electrodes, specifically ERGO/PGE, Ru/ERGO/PGE, Ni/ERGO/PGE and Ru@Ni/ERGO/PGE, were examined using field emission scanning electron microscopy (FESEM) to gain insights into the morphology of the nanoparticles present on their surfaces. The surface of PGE exhibited a flat and irregular topography, as depicted in Fig. 2a. Fig. 2b exhibits the presence of flakes with sheet-like structures that contribute to an uneven surface. The presence of Ru and Ni is

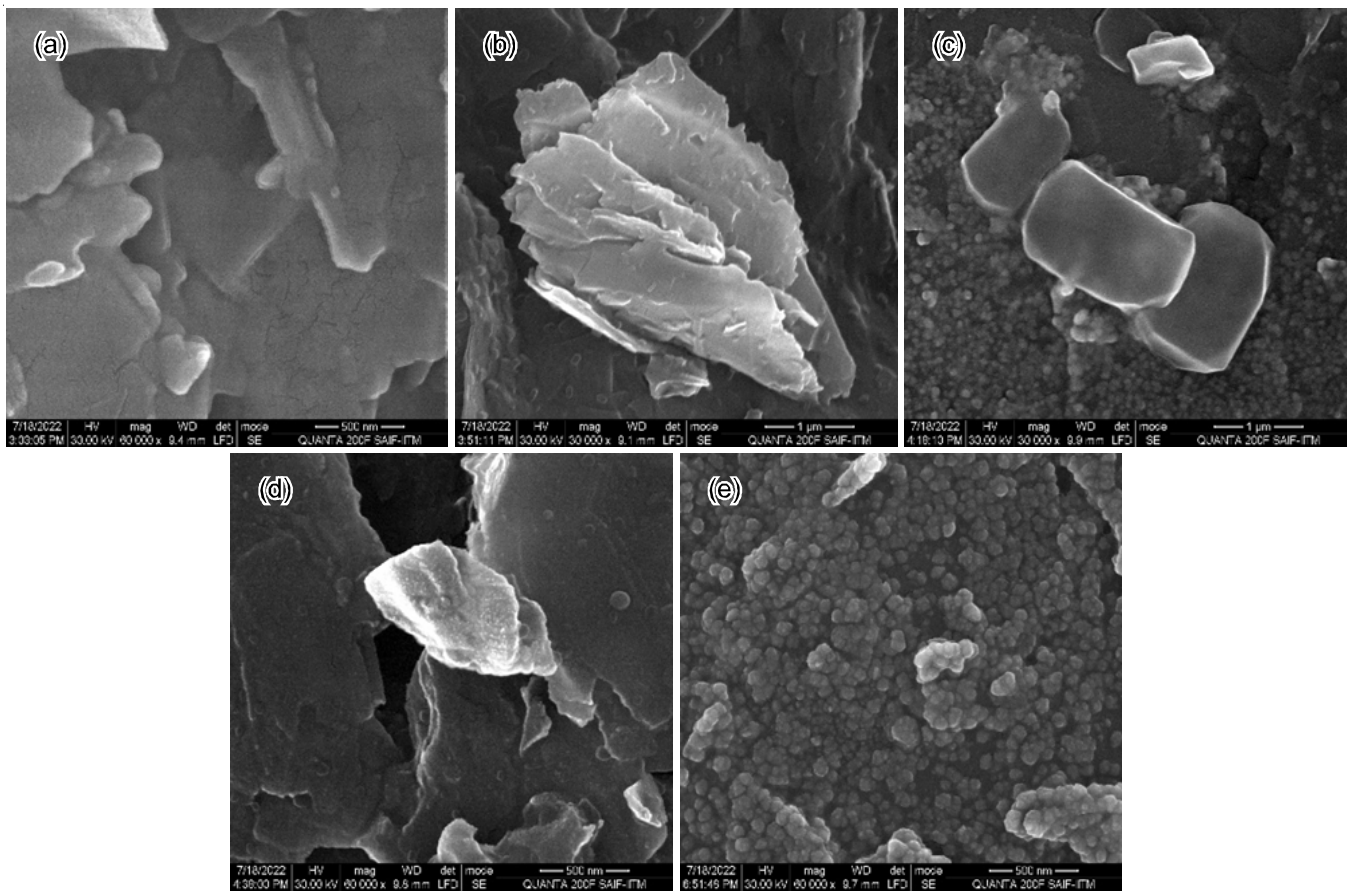

Fig. 2. SEM images of (a) bare PGE, (b) ERGO/PGE, (c) Ru/ERGO/PGE, (d) Ni/ERGO/PGE and (e) Ru@Ni/ERGO/PGE

confirmed in Fig. 2c-d, respectively. The scanning electron microscopy (SEM) images of ruthenium nanoparticles with sizes of 500 nm exhibit cuboid structures. At the resolution of 500 nm, the nickel nanoparticles exhibit a morphology resembling that of a rhomboid. At first glance, the composite material seems like a cluster of grapes (Fig. 2e). The presence of Ru, Ni and Ru@PtNPs is further confirmed by the EDS ratio, as shown in Fig. 3 (inset). The presence of peaks in Fig. 3 corresponds to Ru and Ni in the obtained spectra indicating that the metal nanoparticles were deposited onto the surface of an electrochemically reduced graphene oxide.

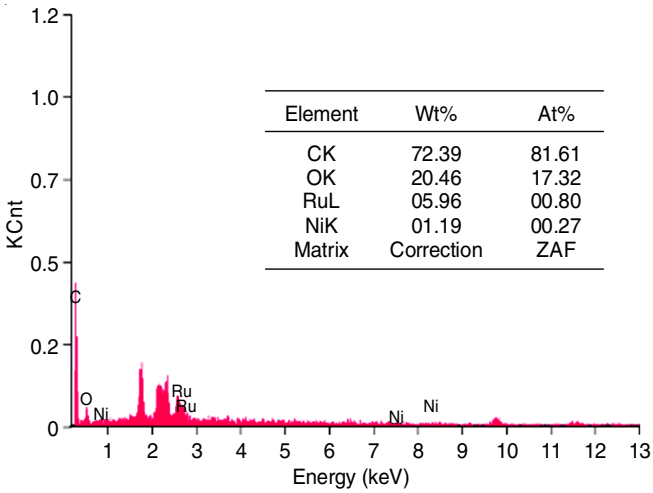

Element	Wt%	At%
CK	72.39	81.61
OK	20.46	17.32
RuL	05.96	00.80
NiK	01.19	00.27
Matrix	Correction	ZAF

Fig. 3. EDS spectrum of Ru@Ni/ERGO/PGE

Electrochemical characterization of Ru@Ni/ERGO/PGE: The electrochemical examination accomplished by cyclic voltammetry and electrochemical impedance spectroscopy to analyze the redox characteristics and electron transfer mechanism of Ru@Ni/ERGO/PGE and other electrodes. The aim of the study was to ascertain the optimal sensing platform for precise determination of the analyte. The cyclic voltammetric measurements were performed using a 5 mM concentration of $[Fe(CN)_6]^{3/4-}$ in a 0.1 M KCl electrolyte. The experiments were conducted within a predetermined potential range of -0.2 to 0.8 V relative to the Ag/AgCl reference electrode. A scan rate of 50 mV/s was utilized. In Fig. 4, a comparative examination of cyclic voltammograms (CVs) acquired from all modified electrodes, in comparison with a pencil graphite electrode (PGE), is presented. The redox behaviour of the composite electrode, which comprises of ruthenium nanoparticles (RuNPs) and nickel nanoparticles (NiNPs) on electrochemically reduced graphene oxide (ERGO) demonstrates superiority. This is supported by the observation of a greater peak current when compared to alternative electrodes. The utilization of Ru/Ni nanoparticles has been observed to augment the efficacy of electron transport through the amplification of the electroactive surface area. The calculation of the electrochemically active surface area was performed using Randle's Sevcik equation (eqn. 2):

$$Ipa = 2.687\times(10)^5\times(n)^{3/2}\times A\times C\times\sqrt{D}\times\sqrt{\partial} \qquad (2)$$

The experimental values obtained from calculating the electroactive surface area of the electrodes were 0.043 cm^2 for PGE, 0.116 cm^2 for ERGO/PGE, 0.117 cm^2 for Ru/ERGO/PGE, 0.171 cm^2 for Ni/ERGO/PGE and 0.173 cm^2 for Ru/Ni/ERGO/PGE. The active surface area of the composite electrode is four times more than bare PGE.

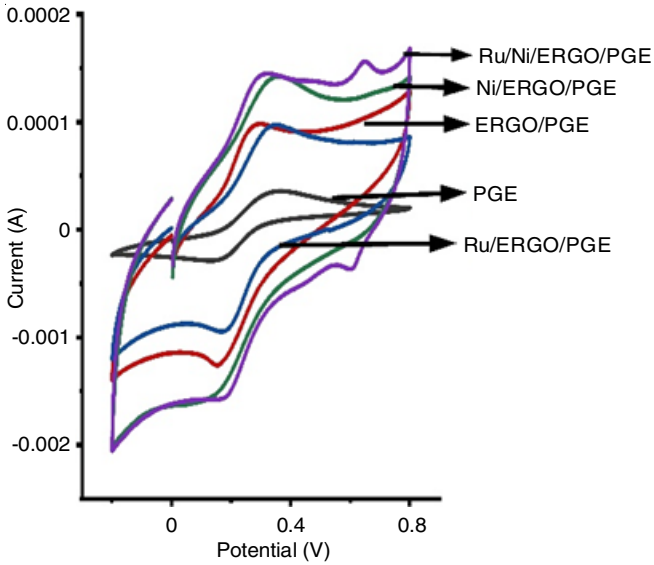

Fig. 4. CV responses of bare PGE, ERGO/PGE, Ru/ERGO/PGE, Ni/ERGO/PGE and Ru/Ni/ERGO/PGE in 5 mM $[Fe(CN)_6]^{3-/4-}$ at 50 mV s^{-1} scan rate

Electrochemical impedance spectroscopy (EIS) studies: Fig. 5 presents the Nyquist plots of various electrodes namely bare PGE, ERGO, Ru/ERGO/PGE, Ni/ERGO/PGE and Ru/Ni/ERGO/PGE nanoparticles. The plots were obtained in a 0.1 M KCl solution containing 5 mM $[Fe(CN)_6]^{3/4-}$ solution. The diameter of the semi-circle in the Nyquist plot corresponds to the charge transfer resistance observed at high frequencies. This indicates that the bare PGE shows the most prominent semi-circle in the high-frequency range, which can be attributed to its elevated resistance (86.342 Ω) to the electron transmission. The electron transfer resistances for the modified electrodes,

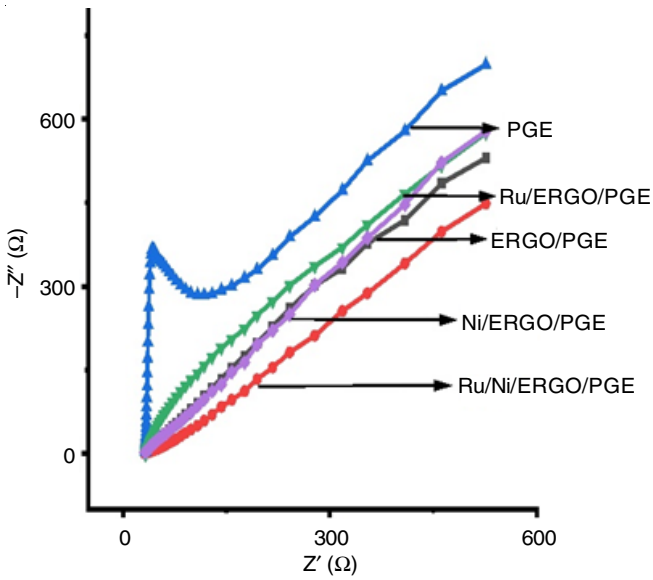

Fig. 5. Nyquist plot of PGE, ERGO/PGE, Ru/ERGO/PGE, Ni/ERGO/PGE and Ru/Ni/ERGO/PGE in 5m M $[Fe(CN)_6]^{3-/4-}$

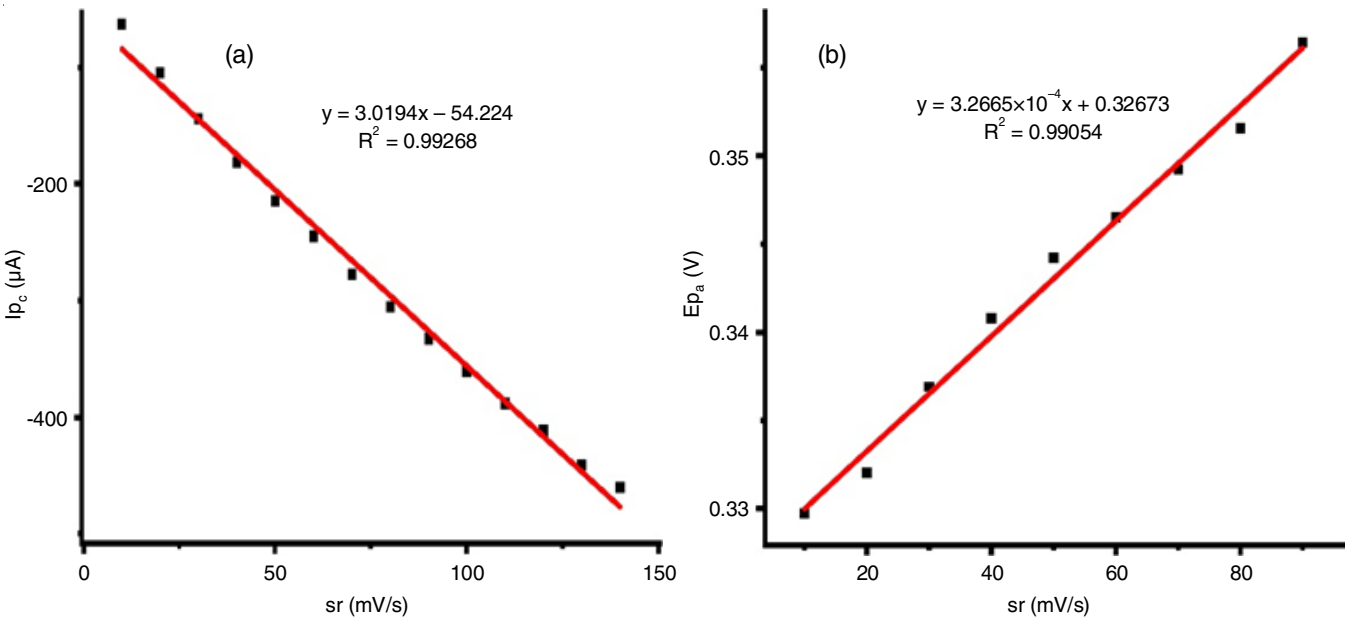

Fig. 6. (a) Calibration plot for Ru/Ni/ERGO/PGE showing the relation between scan rate and cathodic peak current and (b) Calibration plot between scan rate and anodic peak potential

namely bare, ERGO, Ru/ERGO/PGE, Ni/ERGO/PGE and Ru/Ni/ERGO/PGE, were reduced to 65.785, 61.503, 53.432 and 52.124 Ω, respectively. Hence, it becomes evident that the introduction of Ru and Ni onto the surface of electrochemically reduced graphene oxide leads to a reduction in the diameter of the semicircle and an enhancement in electron transmission. This phenomenon can be attributed to the change of the PGE surface. A decrease in R_{ct} can be attributed to the combined effect of the metals, leading to an increase in the electroactive surface area and thus improving the electrical characteristics. Hence, the metal alloy functions as a medium that establishes a connection between the analyte and the transducer, more especially, the working electrode.

Scan rate: The potential varied across different scan speeds, enabling the assessment of the rate at which the applied potential undergoes alteration. An increase in the scan speeds results in a decrease in the size of diffusion layer, which consequently leads to the detection of high currents. The Randles-Sevcik equation establishes that there exists a linear correlation between the peak current and the square root of sweep rate. This equation functions as a means of determining whether a given analyte demonstrates free diffusion within a solution or experiences adsorption onto an electrode. Moreover, the characterization of the analyte's diffusion behaviour can also help in the computation of diffusion coefficients. Fig. 6a presents the findings of a linear regression analysis that was performed to examine the association between the potential scan and the current response Ip_c. The equation resulting from the regression analysis is denoted as Ip_c (μA) = -3.0194ν – 54.224 with a regression of 0.99268. The regression equation depicted in Fig. 6b elucidates the correlation between the scan rate and the peak potential. The expression for Ep_a (V) is given as 3.2665 × 10^{-4} ν + 0.32673, whereas R^2 for this expression was calculated to be 0.99054.

Voltammetric analysis of target analyte

Influence of pH on the determination of *p*-nitrophenol: The supporting electrolyte and its pH have a significant impact on various aspects of voltammograms, including resolution, peak position, intensity, charge transfer and peak current. The analyte is significantly influenced by the pH of the solution. To enhance the efficiency of the peak current response, a study was undertaken to evaluate the impact of several buffers, including phosphate, borate and Britton-Robinson. The phosphate buffer exhibited enhanced performance in terms of both the intensity of the current response and the peak potential attained during the electro-oxidation of *p*-nitrophenol. The presence of a high concentration of hydrogen ions (low pH) makes the *p*-nitrophenol molecule compete with other molecules for electrode surface adsorption sites prior to the electro-oxidation. An increase in pH to a significantly alkaline level (pH 10) causes the separation of *p*-nitrophenol into nitrophenolate anions. At pH 7, the highest current response was once again recorded experimentally. Fig. 7 exhibits the effect of pH on *p*-nitrophenol within the range of 6-10. The noticeable current response was observed only at neutral pH.

The electrochemical performance of both unmodified and modified pencil graphite electrodes (PGEs) was evaluated by the implementation of cyclic voltammetry (CV) analysis. The experiments were evaluated the potential range spanning from +1 to -1 V, with a sweep rate of 50 mV/s. The voltammograms illustrated in Fig. 8 demonstrate the peak current observed at the suggested sensor and the other modified sensors along with bare PGE. The highest peak current is observed at -0.5175 V [29]. The obtained results can be ascribed to the increase in the effective surface area and the decrease in electrical resistance. This work has once again shown evidence for the higher performance of the composite electrode as a sensing platform when compared to monometallic and unmodified electrodes. The

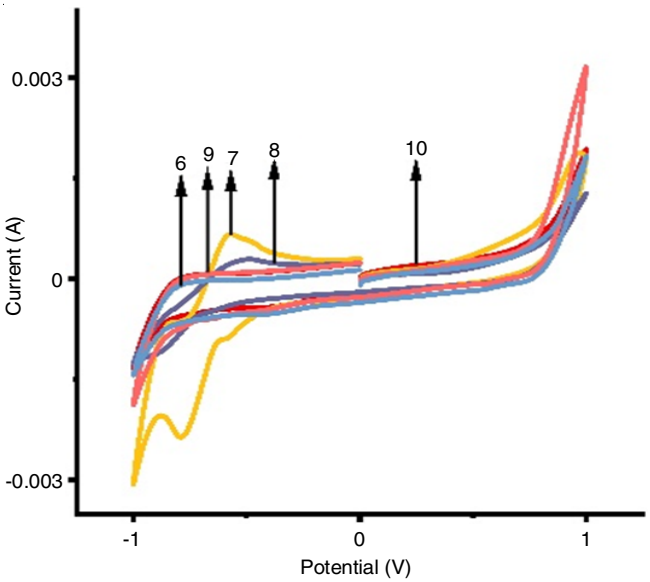

Fig. 7. Effect of pH value of 0.1 M PBS on the current response of 100 µL of 0.01 M PNP at Ru/Ni/ERGO/PGE

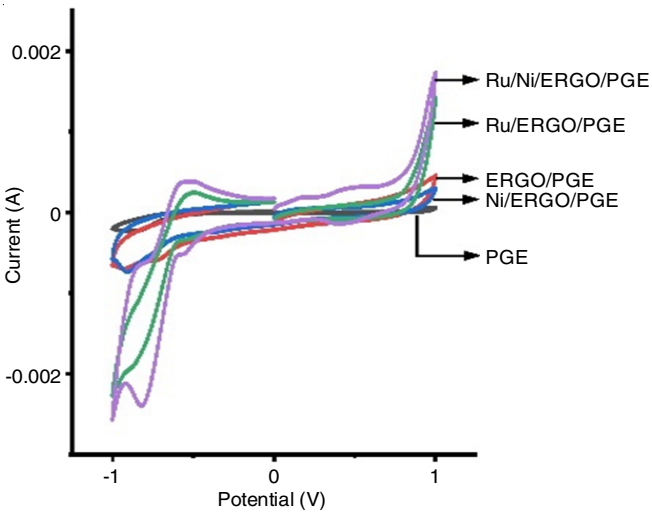

Fig. 8. Comparison of CV responses of bare PGE, ERGO/PGE, Ru/ERGO/PGE, Ni/ERGO/PGE and Ru/Ni/ERGO/PGE in 100 µL of 0.01 M PNA at 50 mV s^{-1} scan rate

electrooxidation of *p*-nitrophenol is enhanced by the inclusion of a composite material consisting of ruthenium nanoparticles (RuNPs), nickel nanoparticles (NiNPs) and electrochemically reduced graphene oxide (ERGO), on a pencil graphite electrode (PGE). This composite material acts as a mediator, effectively amplifying the electrochemical signals. The observed increase in the oxidation current and decrease in the charge transfer resistance, leading to the improved sensitivity of *p*-nitrophenol, can be primarily due to the synergistic interaction between the metals.

The quantification of the electrons involved in the rate determining phase was conducted using eqns. 3 and 4, in accordance with Laviron's equations:

$$Epa = \frac{2.303RT}{2(1-\alpha)n\alpha}\log\nu + k \quad (3)$$

$$Epa = \frac{Ep}{2} = 1.857\left(\frac{RT}{\alpha F}\right) \quad (4)$$

where R is the gas constant, T is the temperature, F represents the Faraday constant and Ep/2 refers to the half-peak potential. The reaction involves the participation of a solitary electron and the measured α value of 0.4245 provides evidence for the method's reversibility. Hence, the electron transfer is more than the mass transfer, thereby making the process diffusion controlled.

Effect of scan rate: The cyclic voltammetry (CV) technique was utilized to examine the electrochemical phenomena at the electrode's surface. To differentiate between a process that is controlled by diffusion and one that is controlled by adsorption, cyclic voltammograms were acquired using various scan rates spanning from 10 to 180 mV/s (Fig. 9). The experimental setup involved the utilization of a composite electrode Ru/Ni/ERGO/PGE. The voltammograms exhibit a clear correlation between the scan rate and the peak current, as observed (Fig. 10). The

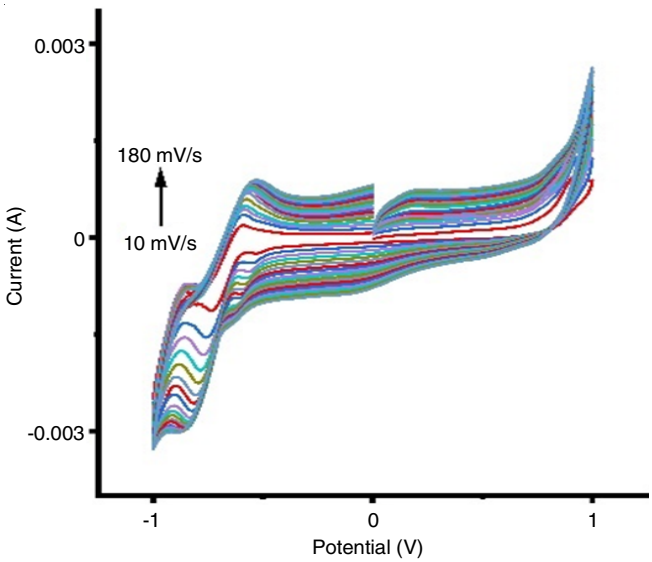

Fig. 9. Influence of scan rate on 100 µL of 0.01 M PNA at Ru/Ni/ERGO/PGE

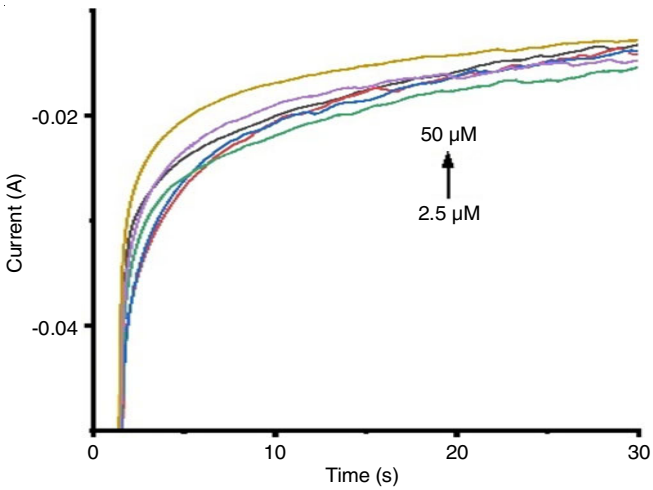

Fig. 10. Chronoamperograms of PNP from 2.5 µM to 50 µM at Ru/Ni/ERGO/PGE

TABLE-1
COMPARISON OF THE DESIGNED SENSOR WITH OTHER REPORTED SENSORS FOR THE DETECTION OF 4-NITROPHENOL

Electrode material	Method	Linearity (M)	LOD (μM)	Stability	Ref.
GCE/Sa/(CTA_{10})	SWV	$0.2 \times 10^{-6} - 6 \times 10^{-6}$	3.5×10^{-2}	–	[15]
PRB/PGE	DPV	$5 \times 10^{-6} - 700 \times 10^{-6}$	1.78	–	[17]
MWNT-Nafion	DPV	$25 \times 10^{-6} - 720 \times 10^{-6}$	3.5	–	[30]
TMA-B	SWV	$0.2 \times 10^{-6} - 200 \times 10^{-6}$	1	–	[5]
Ru@Ni/ERGO/PGE	CA	$2.5 \times 10^{-6} - 50 \times 10^{-6}$	0.36	5 weeks	Present work

relationship between Ip_c (A) and ν can be described by the regression equation: Ip_c (A) = $9.761 \times 10^{-4}\nu + 0.00165$. The coefficient of determination (R^2) for this regression is 0.99198. The linear relationship between scan rate and cathodic peak potential is expressed using a linear equation, specifically $Ep_c = 6.9952 \times 10^{-4}\nu - 0.7459$. The relationship between the variables exhibits a strong match as evidenced by the coefficient of determination (R^2) of 0.9911.

Electrochemical oxidation of *p*-nitrophenol: A 100 μL of 0.01 M *p*-nitrophenol was added to the voltammetric cell, which was already filled with a 38 mL phosphate buffered saline (PBS) solution at pH 7. The electrochemical behaviour of different concentrations of *p*-nitrophenol was investigated using the chronoamperometric technique. Using Cottrell's equation, the diffusion coefficient of analyte was found to be 25.4×10^{-2} cm^2 s^{-1}. The graphical representation in Fig. 11 demonstrates a clear and consistent rise in the maximum current of the sensor after the addition of *p*-nitrophenol. The concentrations of *p*-nitrophenol tested in this experiment spanned from 2.5×10^{-6} M to 50×10^{-6} M. The suggested sensor enables the cathodic oxidation of *p*-nitrophenol to occur within a comparable potential range as that of homologous phenol derivatives. The observed shift of the oxidation peak towards the positive side is a result of the rise in the concentration of *p*-nitrophenol. The linear regression model was employed to determine the equation describing the electrooxidation of *p*-nitrophenol at the electrode composed of. The equation obtained is I (μA) = 4.95×10^{-6} μM – 0.0021 and the coefficient of determination (R^2) for this model was found to be 0.9896. This observation implies that the electrooxidation process is influenced by the electron transport control. The resulting LOD was found to be 0.36 μM. The attained limit of quantification (LOQ) was found to be 1.1×10^{-6} M. It has been observed that in the present work, the LOD was found to be much lower in comparison with the reported methods (Table-1).

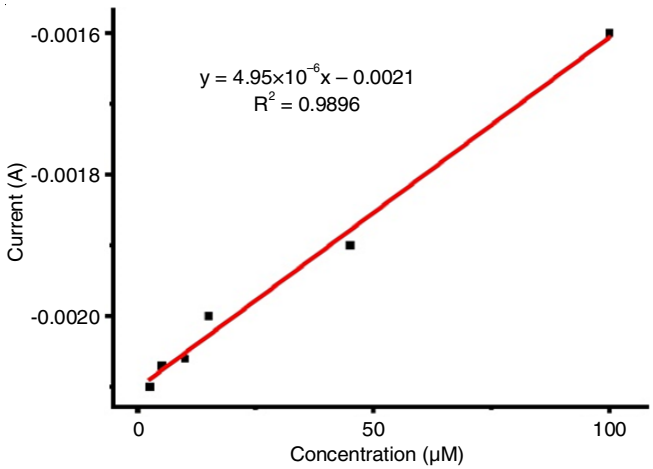

Fig. 11. Fitted regression line plotted between concentration and peak current of PNA

Validity of the proposed sensor: Human caused pesticide degradation was investigated by collecting Buckingham Canal water and soil samples in the agricultural areas of Vaddeswaram village, Guntur city, India. A 5.0 mL of canal water and soil samples were supplemented with different quantities of *p*-nitrophenol and mixed with 34.5 mL of phosphate buffer solution and then sonicated for 5 min. Using differential pulse voltammetry at -0.51 V (against Ag/AgCl), the peak height and oxidation process were observed to quantify the analyte concentration. For repeatability, the experiment was repeated with the same sensor and found an RSD of 2.15%. Sensors were also tested at room temperature after 2-4 weeks of inactivity and found that weekly stability monitoring showed that it retained 94% of its initial value after 5 weeks. The response of sensor in the presence of dopamine, ascorbic acid, paracetamol, *p*-nitroaniline, 4-aminophenol and 2-nitroaniline was selectivite and no interference take place. The proposed method has successfully been tested for the real samples and the results are presented in Table-2.

TABLE-2
DETERMINATION OF 4-NITROPHENOL IN REAL SAMPLES USING THE PROPOSED SENSOR

Sample	Added (mM)	Found (mM)	Recovery (%)
Soil sample	0	0	–
	0.1	0.099	99
	0.2	0.198	99
	0.3	0.301	100.33
Canal water	0	0	–
	0.1	0.101	101
	0.2	0.198	99
	0.3	0.298	99.33

Conclusion

A novel ERGO-based bimetallic nanocomposite as sensing electrode (Ru@Ni/ERGO/PGE) was successfully prepared and employed for the quantification of *p*-nitrophenol at pH 7. The chronoamperometric measurements were investigated as an effective method for the analysis of the electro-oxidation of *p*-nitrophenol. The sensor exhibited a broad linear range that range from 2.5×10^{-6} to 50×10^{-6} M, hence confirmed the capacity to monitor *p*-nitrophenol within the specified interval. In addition, the measurements exhibit a notably low detection limit of 0.36 μM, hence facilitating the highly sensitive detection of *p*-nitrophenol even at extremely low concentrations. The sensor under consideration was successfully employed in the examination of both drinking water and soil samples, exhi-

biting a retention rate of 94% activity even during a 40 day duration of storage at room temperature. Moreover, this material is the first ever bimetallic nanomaterials electrodeposited on PGE-modified ergo. It introduces a novel cost-effective methodology for the detection of *p*-nitrophenol, which involves the electrochemical alteration of pencil graphite using ruthenium-nickel alloy. The determination of the analyte is facilitated by the reduced preparation procedure, enhanced stability, instantaneous detection, applicability to genuine samples, as well as the repeatability and reproducibility of the method.

ACKNOWLEDGEMENTS

The authors are thankful to Koneru Lakshmaiah Education Foundation, Vaddeswaram, Guntur, Andhra Pradesh-522502, India, for providing the necessary laboratory facilities. This work is not financially supported by any funding agencies.

CONFLICT OF INTEREST

The authors declare that there is no conflict of interests regarding the publication of this article.

REFERENCES

1. P. Murugaesan, P. Aravind, N. Guruswamy Muniyandi and S. Kandasamy, *Environ. Technol.*, **36**, 2618 (2015); https://doi.org/10.1080/09593330.2015.1041424
2. B. Ntsendwana, M.G. Peleyeju and O.A. Arotiba, *J. Environ. Sci. Health Part A Tox. Hazard. Subst. Environ. Eng.*, **51**, 571 (2016); https://doi.org/10.1080/10934529.2016.1141623
3. P. Mulchandani, C.M. Hangarter, Y. Lei, W. Chen and A. Mulchandani, *Biosens. Bioelectron.*, **21**, 523 (2005); https://doi.org/10.1016/j.bios.2004.11.011
4. P. Deng, Z. Xu, Y. Feng and J. Li, *Sens. Actuators B Chem.*, **168**, 381 (2012); https://doi.org/10.1016/j.snb.2012.04.041
5. M.J. •unic, A.D. Milutinovic-Nikolic, D.M. Stankovic, D.D. Manojlovic, N.P. Jovic-Jovicic, P.T. Bankovic, Z.D. Mojovic and D.M. Jovanovic, *Appl. Surf. Sci.*, **313**, 440 (2014); https://doi.org/10.1016/j.apsusc.2014.05.228
6. N. Xiao, S.G. Liu, S. Mo, N. Li, Y.J. Ju, Y. Ling, N.B. Li and H.Q. Luo, *Talanta*, **184**, 184 (2018); https://doi.org/10.1016/j.talanta.2018.02.114
7. S. Scarano, P. Palladino, E. Pascale, A. Brittoli and M. Minunni, *Mikrochim. Acta*, **186**, 146 (2019); https://doi.org/10.1007/s00604-019-3259-2
8. B. Wang, P. Liu, Y. Hu, H. Zhao, L. Zheng and Q. Cao, *Dalton Trans.*, **52**, 2309 (2023); https://doi.org/10.1039/D2DT03268F
9. M. Aazza, C. Mounir, H. Ahlafi, A. Bouymajane and F. Cacciola, *J. Mol. Liq.*, **383**, 122139 (2023); https://doi.org/10.1016/j.molliq.2023.122139
10. M.A. Quiroz, C.A. Martínez-Huitle, Y. Meas-Vong, E. Bustos and M. Cerro-Lopez, *J. Electroanal. Chem.*, **807**, 261 (2017); https://doi.org/10.1016/j.jelechem.2017.11.004
11. A.F. Mulaba-Bafubiandi, H. Karimi-Maleh, F. Karimi and M. Rezapour, *J. Mol. Liq.*, **285**, 430 (2019); https://doi.org/10.1016/j.molliq.2019.04.084
12. C. Borras, T. Laredo and B.R. Scharifker, *Electrochim. Acta*, **48**, 2775 (2003); https://doi.org/10.1016/S0013-4686(03)00411-0
13. S. Kalia, R. Kumar, R. Sharma, S. Kumar, D. Singh and R.K. Singh, *J. Phys. Chem. Solids*, **184**, 111719 (2024); https://doi.org/10.1016/j.jpcs.2023.111719
14. T. Yu, K. Herdman, P. Rupa Kasturi and C.B. Breslin, *Microchem. J.*, **195**, 109453 (2023); https://doi.org/10.1016/j.microc.2023.109453
15. G.B.P. Ngassa, I.K. Tonlé and E. Ngameni, *Talanta*, **147**, 547 (2016); https://doi.org/10.1016/j.talanta.2015.10.030
16. E. Alberto, J. Bastos-Arrieta, C. Perez-Rafols, N. Serrano, M.S. Díaz-Cruz and J.M. Díaz-Cruz, *Microchem. J.*, **193**, 109125 (2023); https://doi.org/10.1016/j.microc.2023.109125
17. Sreelekshmi, B. Sajeevan, M.G. Gopika, A.S. Murali, S.M. Senthil Kumar and B. Saraswathyamma, *Mater. Chem. Phys.*, **301**, 127568 (2023); https://doi.org/10.1016/j.matchemphys.2023.127568
18. N. Zalpour and M. Roushani, *Microchem. J.*, **190**, 108750 (2023); https://doi.org/10.1016/j.microc.2023.108750
19. I.G. David, D.-E. Popa and M. Buleandra, *J. Anal. Methods Chem.*, **2017**, 1905968 (2017); https://doi.org/10.1155/2017/1905968
20. W.-W. Liu and A. Aziz, *ACS Omega*, **7**, 33719 (2022); https://doi.org/10.1021/acsomega.2c04099
21. X. Zhu, S. Shi, J. Wei, F. Lv, H. Zhao, J. Kong, Q. He and J. Ni, *Environ. Sci. Technol.*, **41**, 6541 (2007); https://doi.org/10.1021/es070955i
22. S. Kumar, S. Singh and V.C. Srivastava, *Chem. Eng. J.*, **263**, 135 (2015); https://doi.org/10.1016/j.cej.2014.11.051
23. B. Thirumalraj, C. Rajkumar, S.M. Chen and K.Y. Lin, *J. Colloid Interface Sci.*, **499**, 83 (2017); https://doi.org/10.1016/j.jcis.2017.03.088
24. H. Wang, Z. Li, F. Zhang, Y. Wang, X. Zhang, J. Wang and X. He, *Sep. Purif. Technol.*, **266**, 118600 (2021); https://doi.org/10.1016/j.seppur.2021.118600
25. A.L. Lavanya, K.G. Bala Kumari, K.R.S. Prasad and P.K. Brahman, *Int. J. Environ. Anal. Chem.*, **102**, 720 (2022); https://doi.org/10.1080/03067319.2020.1726333
26. S.K. Movahed, P. Jafari and S. Mallakpour, *J. Environ. Chem. Eng.*, **11**, 110426 (2023); https://doi.org/10.1016/j.jece.2023.110426
27. S. Tahtaisleyen, O. Gorduk and Y. Sahin, *Anal. Lett.*, **54**, 394 (2021); https://doi.org/10.1080/00032719.2020.1767120
28. D. Kutyla, K. Kolczyk-Siedlecka, A. Kwiecinska, K. Skibinska, R. Kowalik and P. Zabinski, *J. Solid State Electrochem.*, **23**, 3089 (2019); https://doi.org/10.1007/s10008-019-04374-7
29. K. Barman, B. Changmai and S. Jasimuddin, *Electroanalysis*, **29**, 2780 (2017); https://doi.org/10.1002/elan.201700430
30. A. Arvinte, M. Mahosenaho, M. Pinteala, A.-M. Sesay and V. Virtanen, *Mikrochim. Acta*, **174**, 337 (2011); https://doi.org/10.1007/s00604-011-0628-x